

# Reactive Deposition Versus Strong Electrostatic Adsorption (SEA): A Key to Highly Active Single Atom Co-Catalysts in Photocatalytic H<sub>2</sub> Generation

Yue Wang, Shanshan Qin, Nikita Denisov, Hyesung Kim, Zdeněk Bad'ura, Bidyut Bikash Sarma, and Patrik Schmuki\*

In recent years, the use of single atoms (SAs) has become of a rapidly increasing significance in photocatalytic H<sub>2</sub> generation; here SA noble metals (mainly Pt SAs) can act as highly effective co-catalysts. The classic strategy to decorate oxide semiconductor surfaces with maximally dispersed SAs relies on “strong electrostatic adsorption” (SEA) of suitable noble metal complexes. In the case of TiO<sub>2</sub> – the classic benchmark photocatalyst – SEA calls for adsorption of cationic Pt complexes such as [(NH<sub>3</sub>)<sub>4</sub>Pt]<sup>2+</sup> which then are thermally reacted to surface-bound SAs. While SEA is widely used in literature, in the present work it is shown by a direct comparison that reactive attachment based on the reductive anchoring of SAs, e.g., from hexachloroplatinic(IV) acid (H<sub>2</sub>PtCl<sub>6</sub>) leads directly to SAs in a configuration with a significantly higher specific activity than SAs deposited with SEA – and this at a significantly lower Pt loading and without any thermal post-deposition treatments. Overall, the work demonstrates that the reactive deposition strategy is superior to the classic SEA concept as it provides a direct electronically well-connected SA-anchoring and thus leads to highly active single-atom sites in photocatalysis.

## 1. Introduction

Using supported single atoms (SAs) in catalysis has become a highly investigated topic in heterogeneous catalysis,<sup>[1–5]</sup> electrocatalysis,<sup>[6–10]</sup> and most recently also in photocatalysis.<sup>[11–14]</sup> In classic photocatalytic reactions, a semiconductor is illuminated with super-band-gap light and, as a result, mobile excited charge carriers (i.e., electrons and holes) are generated. These charge carriers then migrate to the semiconductor surface and initiate reduction or oxidation reactions in the environment. One of the most researched reactions is the transfer of photoexcited electrons from the semiconductor conduction band to water or H<sup>+</sup> to produce dihydrogen, H<sub>2</sub>.<sup>[15,16]</sup> On many semiconductor surfaces, this step is kinetically hampered and generally needs to be catalyzed by noble metals such as Pt, Pd, Rh, Au.<sup>[15,17]</sup> The enhanced activity due to these so-called co-catalysts is usually ascribed to: i) a Schottky-type contact formation with the semiconductor that promotes electron transfer via the attached


noble metal, and ii) a facilitated recombination reaction of H<sup>0</sup> species to H<sub>2</sub> (2H<sup>0</sup> → H<sub>2</sub>) – this particularly on Pt, Pd, Rh.<sup>[18–21]</sup> In conventional photocatalysis, the co-catalysts are typically deposited in the form of nanoparticles (crystallites of a few nanometers in diameter) onto the semiconductor surface. In order to minimize the cost of the precious metal and in order to achieve a maximized activity, a substantial body of work targets an optimization of the particle loading and size.<sup>[22–28]</sup> Obviously, a SA state represents a maximized surface-to-volume ratio of a catalytic site and a maximized reactivity, as long as downscaling laws hold.<sup>[29–31]</sup>

A key issue in terms of exploiting SAs is the deposition approach used to establish the SA state on the surface and its stabilization.<sup>[32,33]</sup> The classic and most widely used approach to achieve maximum dispersion of noble metals on many oxides (such as Al<sub>2</sub>O<sub>3</sub>, SiO<sub>2</sub>, TiO<sub>2</sub>) is so-called strong electrostatic adsorption (SEA)<sup>[34–36]</sup> – a term coined by Regalbuto et al.<sup>[37,38]</sup> The technique laid the fundamentals for the preparation of modern supported catalysts and exploiting support interactions following, e.g., Tauster principles.<sup>[39,40]</sup> For TiO<sub>2</sub>, which is not only

Y. Wang, S. Qin, N. Denisov, H. Kim, P. Schmuki  
Department of Materials Science and Engineering  
Chair for Surface Science and Corrosion (WW4-LKO)  
Friedrich-Alexander-Universität Erlangen-Nürnberg  
Martensstraße 7, 91058 Erlangen, Germany  
E-mail: schmuki@ww.uni-erlangen.de

Z. Bad'ura, P. Schmuki  
Regional Centre of Advanced Technologies and Materials  
Šlechtitelů 27, Olomouc 78371, Czech Republic

B. B. Sarma  
Institute of Catalysis Research and Technology and Institute for Chemical  
Technology and Polymer Chemistry  
Karlsruhe Institute of Technology  
76131 Karlsruhe, Germany

 The ORCID identification number(s) for the author(s) of this article can be found under <https://doi.org/10.1002/adma.202211814>

© 2023 The Authors. Advanced Materials published by Wiley-VCH GmbH. This is an open access article under the terms of the Creative Commons Attribution License, which permits use, distribution and reproduction in any medium, provided the original work is properly cited.

DOI: 10.1002/adma.202211814

a classic catalyst-support but also the most studied semiconductor for photocatalytic H<sub>2</sub> generation, a number of SA deposition approaches have been reported<sup>[41–44]</sup> but notably the most recent studies that investigate in detail SAs and their reactivity on TiO<sub>2</sub> supports (e.g.,<sup>[45–47]</sup>) load the Pt SAs using this classic SEA concept. This approach was originally developed by Brunelle,<sup>[48]</sup> Cotescu,<sup>[49]</sup> and Regalbuto<sup>[37,38]</sup> and up to today is considered to be the key strategy in wet noble-metal catalyst loading on an oxide surface. Catalyst preparation usually consists of a wet impregnation step (see, e.g.,<sup>[36,45,46,50,51]</sup>) followed by thermal post-treatments to achieve the active and anchored entity.

Underlying this strategy is that hydroxyl groups that populate oxide surfaces in aqueous solutions become deprotonated and thus negatively charged at a pH value above the point of zero charges (PZC).<sup>[52–54]</sup> As a consequence, at pH values above the PZC of an oxide, the surface would strongly adsorb cations such as tetraamine platinum, [(NH<sub>3</sub>)<sub>4</sub>Pt]<sup>2+</sup> in an alkaline environment.<sup>[54–56]</sup>

In catalytic literature, it is widely perceived that this SEA approach, in general, is superior to other approaches, due to the strong noble-metal attachment and the high loading that can be achieved while maintaining a high metal dispersion.<sup>[53,57,58]</sup> The concept has accordingly been widely used to attach Pt SAs to many substrates, including TiO<sub>2</sub> (see, e.g., reference [45–47]).

In contrast to the SEA strategy, some recent works<sup>[59–69]</sup> used for SAs deposition on TiO<sub>2</sub> nanostructures – including tubes,<sup>[60,61,66]</sup> flakes,<sup>[64,65]</sup> and powders<sup>[67–69]</sup> – an acidic H<sub>2</sub>PtCl<sub>6</sub> precursor solution. In the process, a surface reaction is reported that reduces the Pt<sup>4+</sup> precursor to surface-bound Pt<sup>δ+</sup> SA species where  $\delta \approx 2$  – i.e., in this case, a reductive (thus reactive) deposition of Pt on TiO<sub>2</sub> takes place that we thus want to refer to as SA “reactive deposition” approach.<sup>[62,63,68,70,71]</sup> Some works reported the resulting Pt SAs to be very effective for photocatalytic H<sub>2</sub> generation by such reactive deposition,<sup>[61,65,68]</sup> particularly when deposited from low precursor concentrations (ppm levels).<sup>[67]</sup>

Due to the underlying conceptual opposition to the SEA concept and considering the fundamentally different mechanisms of SEA-based and “reactive” attachment, it is of high scientific and technological interest to evaluate the reactivity differences in the resulting SAs. In this work, we therefore systematically compare Pt SAs loaded titania produced via the classic SEA with “reactive” deposition.

While previous work used nanoscale powders or 3D arrays that provide a large surface area for anchoring SAs and for optimizing the overall performance,<sup>[47,61,67]</sup> for mechanistic studies, they provide a less-than-ideal configuration due to the inherent structural complexity.

Therefore, in the present work, we use direct current (DC) sputter-deposited anatase thin films as the semiconductive platform for photocatalytic H<sub>2</sub> evolution. These compact, flat layers provide a simple and defined geometry for illumination and characterization, in terms of loading and distribution of SAs. The layers were produced and characterized as described previously<sup>[72]</sup> and as briefly given in the Experimental Section.

Overall, we find that a reactive attachment based on hexachloroplatinic(IV) acid (H<sub>2</sub>PtCl<sub>6</sub>) leads directly to SA configuration with a much higher specific activity than achieved with SEA

– and this at a significantly lower Pt loading and without post-deposition treatments.

## 2. Results and Discussion

As mentioned above, as a photocatalytic substrate for our investigations, we use DC sputter deposited anatase layers<sup>[72]</sup> that provide a most straightforward morphology and geometry for illumination as well as characterization of loading and SA distribution. For photocatalytic H<sub>2</sub> evolution measurements, we use these layers in a thickness of 200 nm (described and characterized in previous work<sup>[72]</sup> and in Figure S1, Supporting Information). For transmission electron microscopy (TEM) investigations, 7 nm thick anatase films were used that were fabricated under the same sputter deposition parameters on photolithographically defined TEM supports as described in the Experimental Section and in previous work.<sup>[63]</sup> These layers allow obtaining high-angle annular dark-field scanning transmission electron microscopy (HAADF-STEM) images of the anatase surfaces and atomic resolution for deposited Pt single atoms.

In order to place Pt SAs on the surface via SEA, we followed common literature procedures.<sup>[45,46,73]</sup> For anatase TiO<sub>2</sub> the PZC is  $\approx 5$ –6<sup>[74]</sup> and hence anionic interactions are expected at pH values lower than 5–6 and cationic interactions at pH > 7 (the SEA range). Accordingly, in the first set of experiments, the Pt-SEA-deposition was done using cationic Pt(II) complex from (NH<sub>3</sub>)<sub>4</sub>PtCl<sub>2</sub> at 0.005 mM, 2 mM, and 10 mM at pH = 12.7, i.e., under typical SEA conditions.<sup>[38]</sup> This was compared to the reactive deposition of Pt SAs from an anionic Pt(IV) complex from a very dilute 0.005 mM H<sub>2</sub>PtCl<sub>6</sub> solution (pH = 5.4). For comparison, we also immersed our surfaces in an anionic Pt(II) solution, namely a 0.005 mM (NH<sub>4</sub>)<sub>2</sub>PtCl<sub>4</sub> solution (pH = 5.4).

After immersion and drying, HAADF-STEM images (Figure 1a–c) clearly show that in the reactive case as well as the high and low concentration SEA case, decoration is predominantly present in the form of SAs on the anatase TiO<sub>2</sub> surface (the lattice spacing of 0.35 nm corresponds to the (101) planes of anatase). STEM elemental mapping (Figure S2, Supporting Information) combined with a scanning electron microscope (SEM) confirms the uniform distribution of Pt and the absence of crystallized Pt agglomerates on the surfaces by reactive deposition. While SAs are distinctly present on all treated surfaces, it should be noted, however, that for the 10 mM SEA loading, some SAs are mildly agglomerated to 2D rafts (some examples are marked with orange circles in Figure 1c). From several HAADF-STEM images (examples are provided in Figures S3 and S4, Supporting Information) we performed a detailed evaluation of the size distribution of Pt sites (Figure S5, Supporting Information) and evaluated an average surface site density for each decoration approach. The site density results as: Figure 1 a)  $3.73 \times 10^5 \mu\text{m}^{-2}$  for 0.005 mM H<sub>2</sub>PtCl<sub>6</sub>, b)  $2.73 \times 10^5 \mu\text{m}^{-2}$  for 0.005 mM (NH<sub>3</sub>)<sub>4</sub>PtCl<sub>2</sub>, and c)  $9.40 \times 10^5 \mu\text{m}^{-2}$  for 10 mM (NH<sub>3</sub>)<sub>4</sub>PtCl<sub>2</sub>. I.e., the low concentration reactive and SEA deposition lead to a comparable Pt site density, while the high concentration SEA – to  $\approx 3$  times higher site density (clusters of Pt atoms located in close proximity were treated as single sites). Note also that the reference deposition from a 0.005 mM (NH<sub>4</sub>)<sub>2</sub>PtCl<sub>4</sub> leads to a similar Pt site density of  $1.43 \times 10^5 \mu\text{m}^{-2}$  (Figure S6, Supporting Information). This Pt(II) chlorocomplex

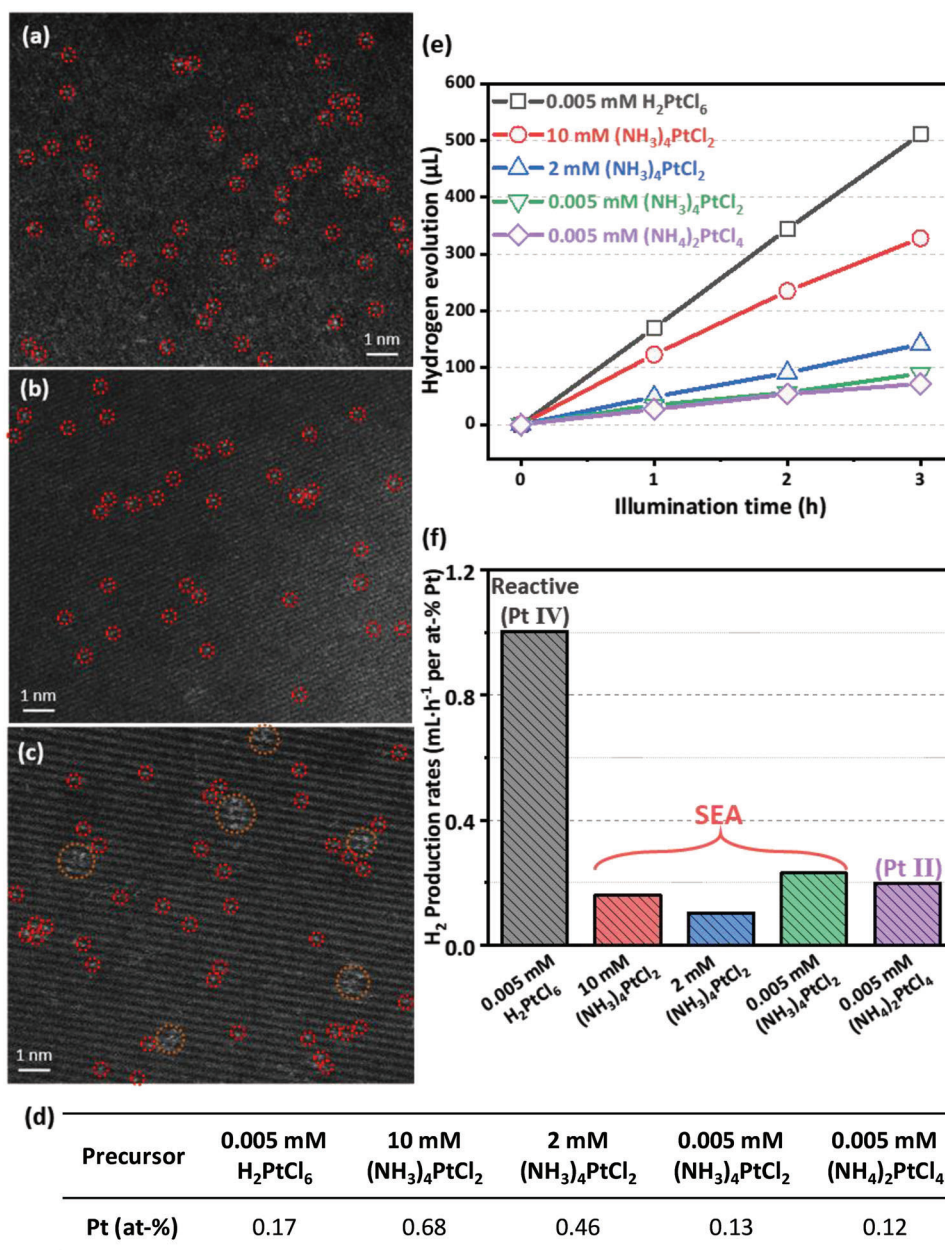


**Figure 1.** HAADF-STEM images of Pt-SA-decorated TiO<sub>2</sub> anatase layers treated in a) 0.005 mM H<sub>2</sub>PtCl<sub>6</sub>, b) 0.005 mM (NH<sub>3</sub>)<sub>4</sub>PtCl<sub>2</sub> and c) 10 mM (NH<sub>3</sub>)<sub>4</sub>PtCl<sub>2</sub>. d) Table of Pt loading on TiO<sub>2</sub> anatase layers prepared by reactive deposition (0.005 mM H<sub>2</sub>PtCl<sub>6</sub> and 0.005 mM (NH<sub>4</sub>)<sub>2</sub>PtCl<sub>4</sub>) and SEA approach (0.005 mM, 2 mM, and 10 mM (NH<sub>3</sub>)<sub>4</sub>PtCl<sub>2</sub> at pH = 12.7). e) Photocatalytic H<sub>2</sub> evolution for the different samples as a function of time. f) Mass-specific H<sub>2</sub> evolution rate for Pt-SA-decorated sputtered layers prepared by reactive deposition and SEA approach.

precursor (NH<sub>4</sub>)<sub>2</sub>PtCl<sub>4</sub> was used with a pH adjusted to match the H<sub>2</sub>PtCl<sub>6</sub> solution, in order to compare the behavior of Pt(IV) and a Pt(II) anionic chloro-complex precursors.

A more averaged quantitative assessment of the Pt loading can be obtained from X-ray photoelectron spectroscopy (XPS). Figure 1d gives a comparison of the loading on the 200 nm thick anatase layers for the SEA and reactive deposition approach (and for some other reference samples). Well in line with TEM, the effective surface loading from different concentrations in the SEA approach range from 0.68 at% (the highest precursor

concentration) to 0.13 at% (the lowest precursor concentration), and the loading from the reactive approach of 0.17 at% is very similar to the lowest concentration of SEA. The (NH<sub>4</sub>)<sub>2</sub>PtCl<sub>4</sub> sample delivered a loading of 0.12 at%, i.e., similar to the loading of the Pt(IV) sample.

Using the SEA approach allows, in line with expectations from literature, to deposit SAs from much higher precursor concentrations than using the reactive approach (the comparison of deposition yields by the two methods is provided in Table S1, Supporting Information) – attempts to use 2 mM H<sub>2</sub>PtCl<sub>6</sub> lead



to relatively stronger aggregation, see e.g., Figure S7 (Supporting Information). For similarly low precursor concentrations, SEA and reactive deposition (at low concentrations) lead both to well-dispersed SAs with a comparable density – this is well in line with expectations from literature.<sup>[61,67,75,76]</sup>

Most remarkable is, however, the different performance of these differently SA-decorated surfaces when tested for photocatalytic H<sub>2</sub> production from a methanol/water solution. Figure 1e shows the amount of photocatalytically produced H<sub>2</sub> over time under a 365 nm LED (65 mW/cm<sup>2</sup>) illumination. From the slopes of the curves in Figure 1e, we obtained the H<sub>2</sub> production rates, and if normalized to the Pt loading (XPS data in Figure 1d), the differences become even more apparent (Figure 1f). Evidently, the far highest H<sub>2</sub> performance is obtained for Pt SAs deposited from the dilute 0.005 mM H<sub>2</sub>PtCl<sub>6</sub> solution with an effective loading of 0.17 at%. The H<sub>2</sub> evolution reaction rate is ≈5 times higher than using SEA with 2000 times higher precursor concentration. Or in other words, the highest Pt surface concentration of 0.68 at% from SEA corresponds to a 4 times higher SA density than from the reactive deposition from H<sub>2</sub>PtCl<sub>6</sub>, nevertheless, the latter reactive deposition approach leads to SAs that show 5 times higher mass-specific activity than deposition using SEA. A similar drastically lower (5 times) reactivity is obtained if SAs are deposited from the Pt(II) precursor (NH<sub>4</sub>)<sub>2</sub>PtCl<sub>4</sub>. This illustrates the strongly more active nature of SAs deposited from the Pt(IV) precursor, see also additional comparisons in Figure S8 (Supporting Information).

**Figure 2a** provides XPS high-resolution spectra of the Pt4f region for the used metal precursors. The corresponding peak fittings are shown in Figure S9 (Supporting Information). In the precursors, clearly, the expected Pt(IV) species with binding energy of Pt4f<sub>7/2</sub> at 75.2 eV (H<sub>2</sub>PtCl<sub>6</sub>) and Pt(II) with binding energy of Pt4f<sub>7/2</sub> at 72.7 eV in (NH<sub>3</sub>)<sub>4</sub>PtCl<sub>2</sub> and in (NH<sub>4</sub>)<sub>2</sub>PtCl<sub>4</sub> can be identified, respectively. Figure 2b shows the Pt4f spectra for TiO<sub>2</sub> surfaces loaded with Pt SAs using different precursors. After reactive attachment, the chemical state of the SAs is Pt<sup>δ+</sup> with a nominal charge of δ ≈ 2, consistent with our previous works.<sup>[62,63,68]</sup> I.e., in the attachment process, the Pt(IV) precursor reacts to a surface coordinated Pt<sup>δ+</sup> state. For (NH<sub>4</sub>)<sub>2</sub>PtCl<sub>4</sub> and (NH<sub>3</sub>)<sub>4</sub>PtCl<sub>2</sub>, the initial Pt(II) state is observed also after surface adsorption for 10 mM, 2 mM, and 0.005 mM loadings. From the N1s peak in Figure 2c it is apparent that for the amine complex, the N coordination to Pt is largely maintained. This is particularly evident for the higher precursor concentrations where an N to Pt ratio of 3–4: 1 can be extracted (Table S2, Supporting Information) – this is well in line with an attachment of the intact [(NH<sub>3</sub>)<sub>4</sub>Pt]<sup>2+</sup> complex for the (NH<sub>3</sub>)<sub>4</sub>PtCl<sub>2</sub> precursor.

But this is in stark contrast to the H<sub>2</sub>PtCl<sub>6</sub> precursor for reactive deposition; in this case, not only the Pt has reacted from Pt(IV) to Pt(II), but also in the attachment reaction, the Cl<sup>-</sup> coordination is entirely lost (Figure 2d). For the H<sub>2</sub>PtCl<sub>6</sub>, the attachment reaction – in agreement with literature – leads to surface coordination of Pt<sup>δ+</sup> SAs coordinated with surface oxygen.<sup>[63,67]</sup>

The fundamental difference in the attachment is easily visible in electronic paramagnetic resonance (EPR) spectra shown in Figure 2e,f for powdered reference samples (only powders allow for sufficiently accurate EPR measurements). The signature consists of a response at g = 1.98 and at g ≈ 1.95 that can be ascribed

to titania-oxygen vacancies (Ti<sup>3+</sup>-O<sub>v</sub>) embedded in the lattice and to surface-exposed Ti<sup>3+</sup>-O<sub>v</sub> states, respectively.<sup>[77–79]</sup>

Evidently, SEA only mildly alters this EPR signature (in line with SEA literature<sup>[45]</sup>). In contrast, reactive deposition leads to a significant decrease in the surface Ti<sup>3+</sup> signature (in line with related work<sup>[60,61,63]</sup>) – this is a direct consequence of Ti<sup>3+</sup> reaction with a Pt<sup>4+</sup> precursor species in a galvanic displacement reaction (Pt<sup>4+</sup> + 2Ti<sup>3+</sup> → Pt<sup>2+</sup> + 2Ti<sup>4+</sup>). Additionally, only in the EPR spectra after reactive deposition, a strong signal corresponding to paramagnetic Pt<sup>+</sup>/Pt<sup>3+</sup> cations (g ≈ 2.15)<sup>[80]</sup> can be detected. This has been previously ascribed to electronic coupling of Pt<sup>2+</sup> sites with oxide support.<sup>[81]</sup> The fact that the Pt<sup>+</sup>/Pt<sup>3+</sup> signal does not appear after SEA deposition signifies the absence of such a coupling.

We further performed X-ray absorption spectroscopy (XAS) measurements for Pt SAs species produced by SEA and reactive deposition approaches (Figure S10, Supporting Information). The X-ray absorption near edge structure (XANES) spectra confirm the presence of positively charged Pt centers (Pt<sup>δ+</sup>) in both samples (Figure S10a, Supporting Information), and X-ray absorption fine structure (EXAFS) analysis shows for both samples a very similar radial distribution function (Figure S10b, Supporting Information) with a maximum signal at 1.59–1.63 Å. This can be expected as Pt<sup>2+</sup> in a Pt–N coordination (SEA) and in Pt–O coordination have very similar coordination lengths.<sup>[82,83]</sup>

Generally, a reactive deposition can also indirectly be observed from UV–vis spectra (Figure S11, Supporting Information). Please also note that hydrolysis of the precursor H<sub>2</sub>PtCl<sub>6</sub> is the key to the formation of the active coupling agent. I.e., in the most active state of a 0.005 mM H<sub>2</sub>PtCl<sub>6</sub><sup>[84]</sup> solution Pt(Cl)<sub>x</sub>(OH)<sub>y</sub>(H<sub>2</sub>O)<sub>z</sub> species are present<sup>[85–89]</sup> – with increasing dilution, OH<sup>-</sup> and water ligands become dominant<sup>[85]</sup> – this is key to the loss of Cl species in the reaction. If we suppress Cl<sup>-</sup> and OH<sup>-</sup> ligand exchange, by adding NaCl or HCl to the precursor, surface uptake of Pt and SA-reactivity are strongly suppressed (see Figure S12, Supporting Information).

The most distinctive difference between reactive deposition and SEA is apparent in linear sweep voltammetry (LSV) measurements. These measurements were carried out to compare the electron transfer properties of Pt SAs sites produced by reactive deposition and SEA, as shown in Figure 2g. As compared to bare TiO<sub>2</sub>, both Pt SAs deposition approaches lead to significant cathodic current densities owing to the electron transfer via Pt SAs sites. Evidently, reactive deposition of the Pt SAs provides a much better charge transfer for a nearly identical Pt loading (0.73 at% Pt by reactive deposition using 2 mM H<sub>2</sub>PtCl<sub>6</sub>, and 0.68 at% Pt by SEA using 10 mM (NH<sub>3</sub>)<sub>4</sub>PtCl<sub>2</sub>). The unique Pt anchoring provided by reactive deposition, which in turn facilitates electron transfer, can thus explain the superior co-catalytic performance of “reactively” deposited Pt SAs.

One factor for the inferior charge transfer and thus the comparably low photocatalytic activity may be due to the fact that in SEA approach still an amino-coordinated Pt complex is attached.

The inferior anchoring of SAs deposited by SEA is also apparent in cyanide leaching experiments (see Figure S13, Supporting Information). While for SAs prepared using reactive deposition show hardly any loss of Pt under the used leaching conditions, 1.17 at% of the SEA deposited Pt is lost under the same conditions.

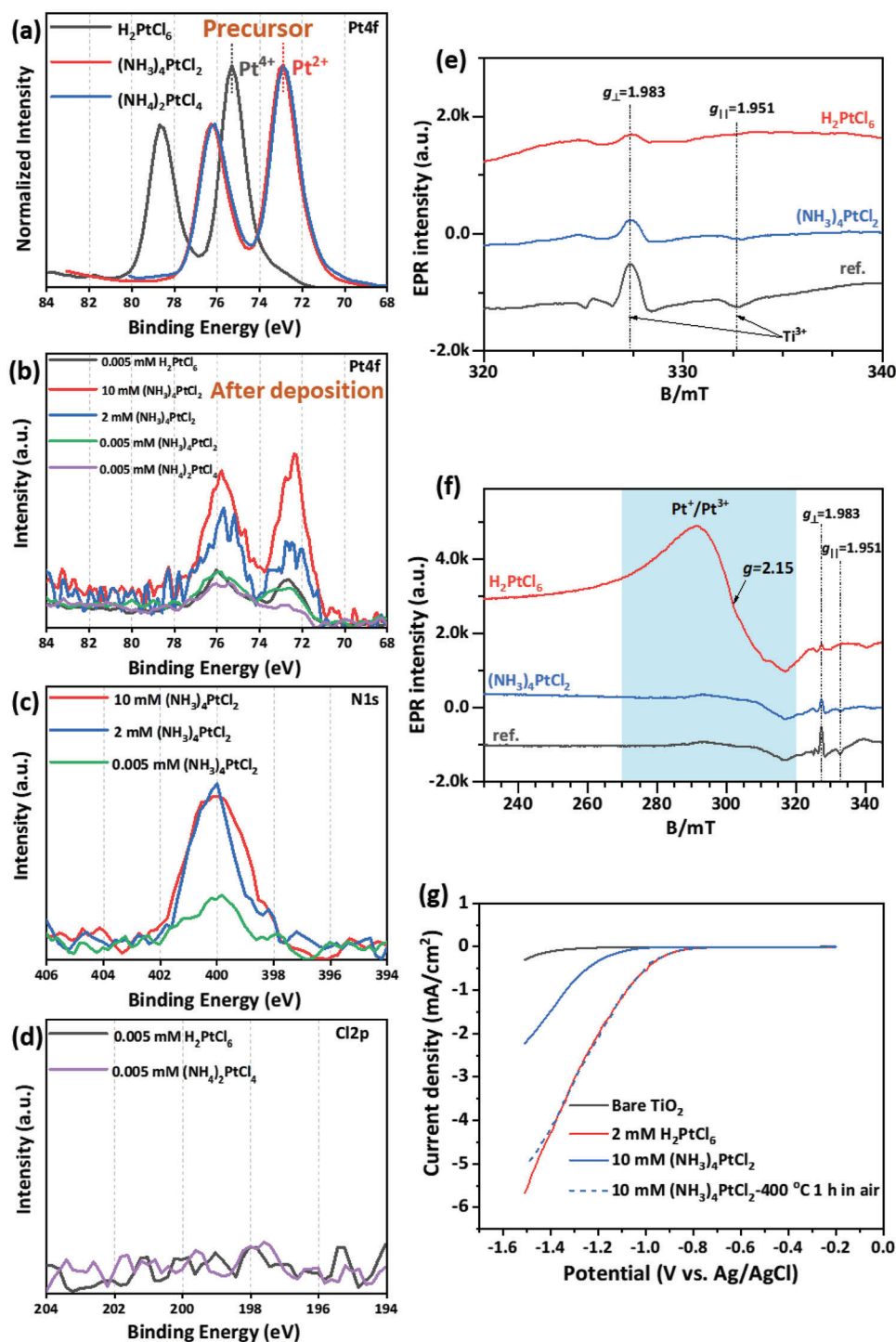


**Figure 2.** a) XPS Pt4f spectra of different Pt precursor salts. b) XPS Pt4f spectra of sputtered TiO<sub>2</sub> anatase layers treated in different precursors. c) XPS N1s spectra of TiO<sub>2</sub> anatase layers treated in  $(\text{NH}_3)_4\text{PtCl}_2$  with different concentrations. d) XPS Cl2p spectra of TiO<sub>2</sub> anatase layers treated in 0.005 mM  $\text{H}_2\text{PtCl}_6$  and 0.005 mM  $(\text{NH}_4)_2\text{PtCl}_4$ . e, f) EPR spectra of anatase TiO<sub>2</sub> nanosheets before (Reference) and after Pt SAs deposition by reactive (in 0.005 mM  $\text{H}_2\text{PtCl}_6$ ) or SEA (in 10 mM  $(\text{NH}_3)_4\text{PtCl}_2$ ) approach ((e) is amplified at 320 mT–340 mT from (f)). g) LSV curves of bare TiO<sub>2</sub> anatase layers, and after Pt SAs deposition via reactive (2 mM  $\text{H}_2\text{PtCl}_6$ ) or SEA (10 mM  $(\text{NH}_3)_4\text{PtCl}_2$ ) approach. For SEA deposition, the curve after heat treatment at 400 °C in air is additionally shown.

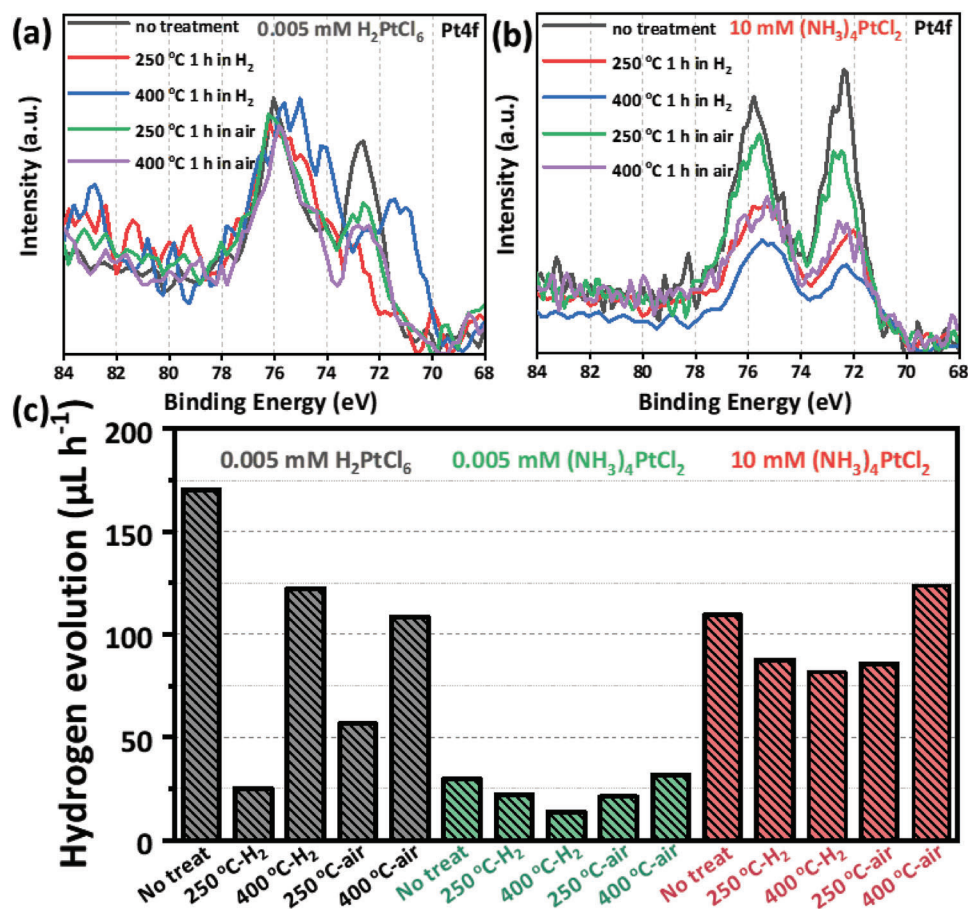


**Figure 3.** XPS Pt4f spectra of TiO<sub>2</sub> anatase layers deposited in a) 0.005 mM H<sub>2</sub>PtCl<sub>6</sub> and b) 10 mM (NH<sub>3</sub>)<sub>4</sub>PtCl<sub>2</sub>, and treated under different annealing conditions. c) Photocatalytic H<sub>2</sub> evolution rate of Pt-SA-decorated sputtered layers treated under different annealing conditions.

In classic SEA approaches, after precursor adsorption, an additional thermal treatment or thermal reduction step is applied, commonly in air or in H<sub>2</sub> environment at elevated temperatures.<sup>[45–47,53,57,73]</sup> The goal is to reduce/react the attached Pt-ions or complexes to surface-anchored Pt species. Heat treatments, however, have been reported to be (partially) detrimental to an atomic dispersion of the Pt species.<sup>[34,37]</sup> In the present work, to address a variety of such preparation steps, we investigate the activity of the different attachment strategies also after additional thermal air or H<sub>2</sub>-reduction treatments (we use conditions commonly used in literature<sup>[45–47,53,57,73]</sup>). More precisely, we treated all samples obtained either by SEA from a 10 mM Pt solution ((NH<sub>3</sub>)<sub>4</sub>PtCl<sub>2</sub>) or by reactive deposition from the 0.005 mM H<sub>2</sub>PtCl<sub>6</sub> solution in H<sub>2</sub> at 250 °C and 400 °C as well as in air at 250 °C and 400 °C. **Figure 3a,b** shows XPS Pt4f peaks after annealing the reactive deposition and SEA samples in air and in H<sub>2</sub> under different conditions. Evidently, after annealing in H<sub>2</sub> for both samples, a partial reduction is observed. The corresponding peak fittings are shown in Figures S14 and S15 (Supporting Information). The Pt4f peak at 72.6 eV for oxygen-coordinated Pt<sup>δ+</sup> is shifted to a position of 71–72 eV. Please note that this position is still higher than the typical 70.5 eV for metallic Pt<sup>0</sup>.<sup>[67]</sup> The Cl2p region in case of TiO<sub>2</sub> anatase layers deposited in 0.005 mM H<sub>2</sub>PtCl<sub>6</sub> and treated under

different annealing conditions shows only noise (Figure S16a, Supporting Information) – the latter indicates that the Pt signals originate from surface-trapped Pt rather than from surface-adsorbed Pt-chloro-complexes (split of the chloro-coordinated precursor Pt species when reacting with the surface).

This reduction does not occur to this extent for air annealing of either type of sample (SEA and reactive). Noteworthy is that the nitrogen coordination sphere for the SEA sample is partially lost in air at 250 °C and almost completely at 400 °C, as evident from the XPS N1s region shown in Figure S16b (Supporting Information). The corresponding peak fittings are shown in Figure S17 (Supporting Information).

Figure 3c shows the photocatalytic H<sub>2</sub> production activity for the different samples. For the SEA samples, the heat treatment in general has less of an influence on the activity than for the reactively Pt-deposited samples, but it is notable that the activity for the SEA samples is slightly increased after some heat treatments (a similar trend is also observed at lower Pt loading, Figure S18, Supporting Information). Note that after heat treatment, the inferior charge transfer of SEA can be largely remediated (see LSV in Figure 2g). But most remarkably, still reactive deposition from H<sub>2</sub>PtCl<sub>6</sub> without any post-treatment shows the highest reactivity. I.e., in the case of reactive deposition, all thermal treatments are at least partially detrimental. In fact, for the reactive deposi-



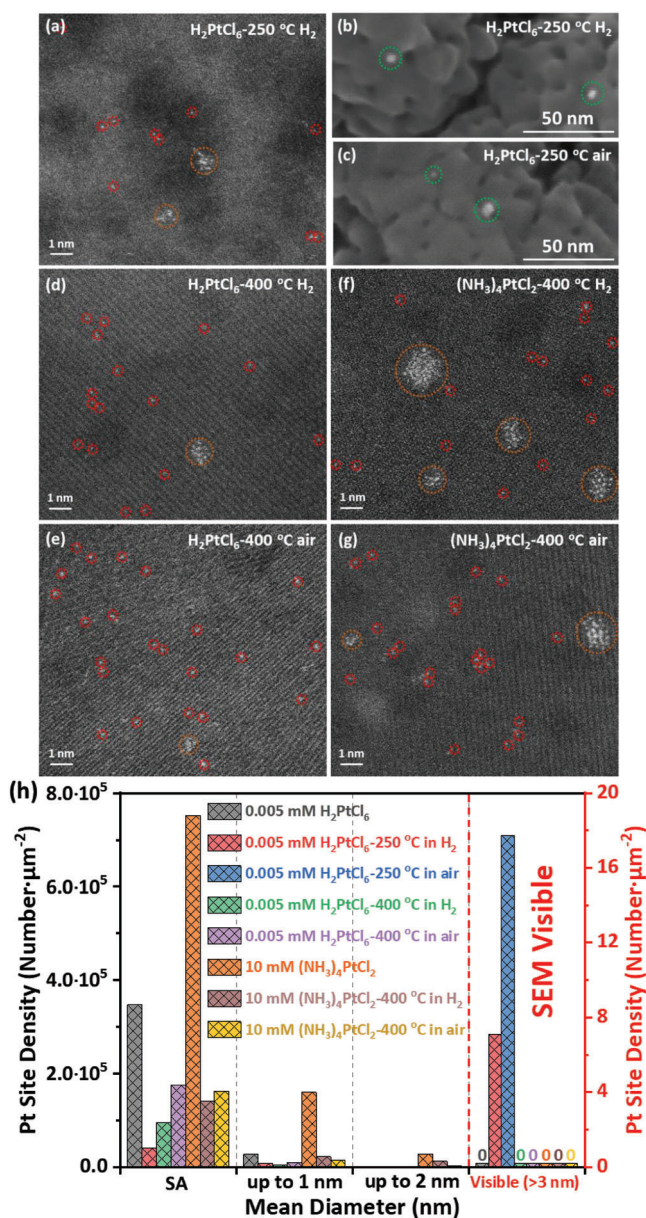


**Figure 4.** a–e) HAADF-STEM images and SEM images of TiO<sub>2</sub> anatase layer deposited in 0.005 mM H<sub>2</sub>PtCl<sub>6</sub> and treated under different annealing conditions. f,g) HAADF-STEM images of TiO<sub>2</sub> anatase layer deposited in 10 mM (NH<sub>3</sub>)<sub>4</sub>PtCl<sub>2</sub> and treated under different annealing conditions. h) Statistics of size distribution percentage of agglomerates for Pt-SA-decorated sputtered layers treated under different annealing conditions.

tion, a drastic drop of the activity after annealing at 250 °C in H<sub>2</sub> or air is observed while annealing at 400 °C recovers the activity strongly.

In view of these effects, we examined the annealed samples in HAADF-STEM and SEM. **Figure 4a–g** shows the reactive and SEA deposited samples after different thermal treatments. In all cases, a partial thermal agglomeration of the single atoms, namely to 2D rafts or even 3D structures occurs. Nevertheless, in all cases still numerous individual SAs are left. An evaluation of Pt size distribution obtained from several HAADF-STEM (ex-

amples are provided in Figures S19 and S20, Supporting Information) and SEM images are shown in Figure 4h. As expected, for the annealed samples, thermally induced agglomeration leads to a broadened size distribution of Pt sites, agglomerate sizes (mainly 2D rafts) reach 2 nm, but SAs still constitute 50–80% of surface Pt sites (Pt nanoparticles and clusters of Pt atoms located in close proximity were treated as single sites). The Pt site density decreases by 2.0–7.9 times (0.005 mM H<sub>2</sub>PtCl<sub>6</sub>-deposited sample) or by 5.2–5.4 times (10 mM SEA-deposited sample). Most interestingly, for the samples annealed at 250 °C (air and H<sub>2</sub>), large agglomerates (visible in SEM) can be found (Figure 4b,c) – this at a very low site density. This strong agglomeration is the most plausible reason for the low activity for photocatalytic H<sub>2</sub> evolution of the reactive samples annealed at 250 °C. In contrast, after 400 °C annealing (in air and H<sub>2</sub>), there are no large agglomerates detectable anymore by SEM (Figure S21, Supporting Information). From HAADF-STEM the Pt site density increases from  $0.48 \times 10^5 \mu\text{m}^{-2}$  at 250 °C to  $1.85 \times 10^5 \mu\text{m}^{-2}$  at 400 °C.

This on the first sight surprising finding can be rationalized in the light of studies on thermal stability of Pt on TiO<sub>2</sub><sup>[90–93]</sup> and other surfaces.<sup>[94]</sup> These reports find that a thermal redispersion of agglomerates, namely NPs to SAs becomes possible at temperatures as low as 400 °C in various atmospheres. Depending on the nature of the support and the atmosphere composition, different mechanisms for Pt redispersion have been suggested, such as reoxidation of amorphous clusters,<sup>[45]</sup> molecular migration of Pt oxide,<sup>[91]</sup> reverse oxygen spillover from Ti<sup>4+</sup> to Pt,<sup>[90]</sup> or anchoring to oxygen vacancy sites.<sup>[92]</sup> In contrast to H<sub>2</sub>PtCl<sub>6</sub>, for SEA-deposited sample, agglomeration in contrast to the as-deposited situation decreases the Pt site density from  $9.40 \times 10^5 \mu\text{m}^{-2}$  to  $1.75 \times 10^5 \mu\text{m}^{-2}$ , but for the different annealing temperatures, a similar Pt site density ( $1.75\text{--}1.8 \times 10^5 \mu\text{m}^{-2}$ ) is observed regardless of the heating atmosphere (400 °C in air or H<sub>2</sub>). Also, there are no large agglomerates detectable by SEM (Figure S22, Supporting Information) for all different annealing conditions.

In view of the efficiency of Pt use, it is interesting to normalize the data in Figure 3c by the Pt loading. The Pt loading for all samples determined by XPS is given in **Figure 5a** and the accordingly normalized activity data in Figure 5b.

The compilation in Figure 5b shows that the individual SAs deposited by reactive deposition leads to  $\approx 5\text{--}6$  times higher activity than the SAs deposited by SEA without thermal treatment and  $\approx 3$  times higher than SEA with a “best” thermal treatment. This shows the significant advantage of a SA decoration using an H<sub>2</sub>PtCl<sub>6</sub> precursor in comparison to the (NH<sub>3</sub>)<sub>4</sub>PtCl<sub>2</sub> precursor. It should also be noted that in recent papers we have shown that agglomeration of Pt SAs on TiO<sub>2</sub> surfaces can occur under photocatalytic conditions.<sup>[84,95]</sup> Here we also provide a post-catalytic characterization of the thermally-treated samples (Figure S23, Supporting Information), which shows the presence of both Pt nanoparticles and abundant single-atom sites on the surface. It is, however, important that agglomerated SAs (to nanoparticles) do not really contribute to the reactivity.<sup>[68]</sup> And thus, light-induced agglomeration does not lead to a decrease in activity.<sup>[68,84,95]</sup> The remaining SAs can provide the entire reactivity under standard illumination conditions.<sup>[68,84]</sup> Nevertheless it cannot be fully excluded that light-induced agglomeration is slightly different for the two deposition processes and thus may

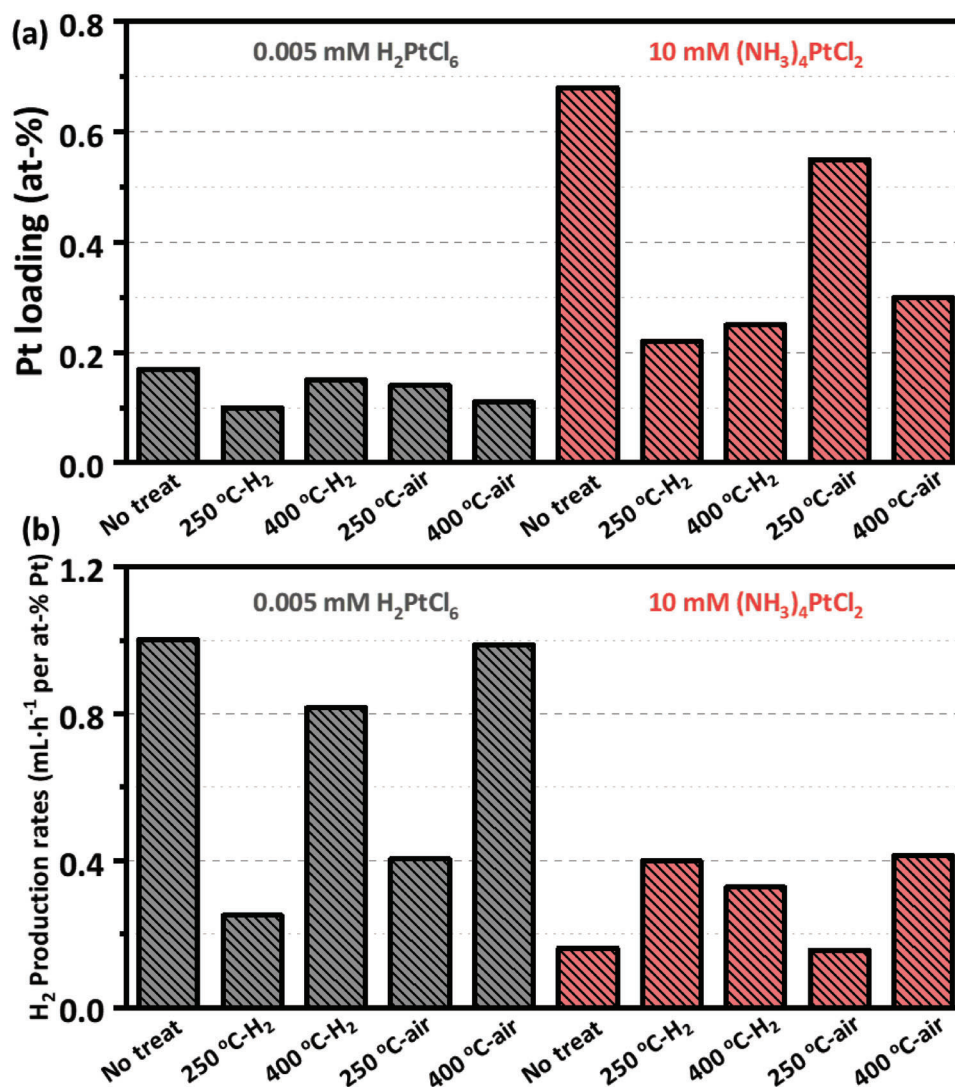


**Figure 5.** a) Pt loading on TiO<sub>2</sub> anatase layers deposited in 0.005 mM H<sub>2</sub>PtCl<sub>6</sub> and 10 mM (NH<sub>4</sub>)<sub>2</sub>PtCl<sub>2</sub> and treated under different annealing conditions determined from XPS data. b) Mass-specific photocatalytic H<sub>2</sub> evolution rate for Pt-SA-decorated sputtered layers treated under different annealing conditions.

contribute to the observed results (however the overall statement about the performance of the two approaches remains unaffected – at least over the investigated time scale).

Noteworthy are also some other reference experiments. If we use SEA at a lower pH 10 as sometimes employed in literature,<sup>[46]</sup> we obtain even a lower reactivity (Figure S8, Supporting Information) than for pH 12.7 which may be ascribed (using the classic Regalbuto-model) to the insufficient negative charge on the TiO<sub>2</sub> at this pH. If we use H<sub>2</sub>PtCl<sub>6</sub> at similar precursor concentrations, i.e., at 2 mM or 10 mM, a significantly lower activity is observed (Figure S8, Supporting Information). Using (NH<sub>4</sub>)<sub>2</sub>PtCl<sub>6</sub> (i.e., another Pt(IV) salt) as a reactive precursor, we also obtain the high reactivity features of reactive deposition from H<sub>2</sub>PtCl<sub>6</sub> (Figure S8, Supporting Information). Together with the finding of (NH<sub>4</sub>)<sub>2</sub>PtCl<sub>2</sub> – the Pt(II) salt of the same precursor – the crucial role of the surface reduction process from Pt(IV) to Pt(II) to create strongly active sites becomes

evident. One may deduce that the process is self-homing (self-creates the most active sites) in the sense that reaction takes place on the surface at active locations, which in turn are also the most active for photocatalytic H<sub>2</sub> generation. This may be put in the context of recent work on the catalytic oxidation of CO that showed that the activity of Pt SAs anchored on TiO<sub>2</sub> is highly dependent on the specific site of Pt-surface coordination. It was reported that highly coordinated Pt SAs,<sup>[45,47]</sup> e.g., in Ti5c or 6c positions, show a significantly lower reactivity than more loosely SAs coordinated at surface step edges and terraces (that nominally are PtOH species or other lower oxygen coordinated species<sup>[47]</sup>).

Following the same arguments, one may thus stipulate that the sites where reductive attachment occurs are provided by specific surface sites which then also provide the highest reactivity in the photocatalytic reaction. Nevertheless, a key difference to “chemical catalysis” is that in photocatalysis the charge transfer



from the substrate to the co-catalyst is essential and can be the rate-determining factor.

### 3. Conclusions

The present work clearly shows that reactive deposition on titania surfaces using diluted  $\text{H}_2\text{PtCl}_6$  or similar Pt(IV) complexes leads directly after surface interaction to a more active configuration than classic strategies using SEA. Even when common heat treatments (and activation) of the SEA complexes are carried out in air or  $\text{H}_2$ , not the same level of co-catalytic activity can be provided.

A significant difference in the adsorption of  $\text{H}_2\text{PtCl}_6$  and  $(\text{NH}_3)_4\text{PtCl}_2$  is that in the former one, the chloride coordination sphere is entirely lost while the nitrogen sphere (from ammonia) is still (partially) present. Moreover, in the attachment process, a reduction from  $\text{Pt}^{4+}$  to  $\text{Pt}^{2+}$  takes place – i.e., a reactive deposition of the Pt SAs takes place.<sup>[61–63]</sup> Such a reactive attachment is in line with  $\text{H}_2\text{PtCl}_6$  coupling to alumina surfaces at low pH<sup>[96–99]</sup> where a ligand exchange type of anchoring was found.

The reactive species is a well-hydrolyzed intermediate, most likely  $[\text{PtCl}_3(\text{OH})_3]^{2-}$ ,<sup>[89]</sup> or even further hydrolyzed species. In the case of  $\text{TiO}_2$ , reductive reaction occurs via an interaction with surface  $\text{Ti}^{3+}$  species of  $\text{TiO}_2$  (accompanied by a complete loss of Cl ligands). Thus produced  $\text{Pt}^{2+}$  species can attach to surface terminal groups of  $\text{TiO}_2$  (e.g., Ti-OH) via Pt-O-Ti or Ti-O-Pt-O-Ti coordination.<sup>[83,100]</sup>

Moreover, while for reactive deposition any heat treatment is detrimental for the photocatalytic activity, in the case of SEA, heat treatments are generally mildly beneficial – this seems to be due to a loss of  $\text{NH}_3$ -coordination, but possibly, even more, it can be ascribed to the entirely different attachment of the Pt species, which significantly affects electron transfer via these sites. While SEA is expected to lead, to a large extent, to randomly attached  $[(\text{NH}_3)_4\text{Pt}]^{2+}$ -complexes that then in a later step are reacted to randomly attached Pt SAs, the reactive deposition takes place likely at preferentially reactive sites. I.e., the Pt SAs react at specific surface sites, which then provide, directly a surface configuration of high activity.

It should be noted, however, that photocatalytic activity is not necessarily equal to catalytic activity for the  $\text{H}_2$  formation reaction, as in photocatalysis also the transfer of a photoexcited electron across the  $\text{TiO}_2$ /Pt interface may be key – and thus the origin of a high reactivity at a specific site in photocatalysis may have underlying different reasons than active spot in classic, “electroless” catalysis.

### 4. Experimental Section

**Materials:** Methanol (99.9%, Carl Roth), ethanol (99.8%, Carl Roth),  $\text{H}_2\text{PtCl}_6 \cdot 6\text{H}_2\text{O}$  (40.17% metallic Pt weight concentration, Metakem),  $(\text{NH}_3)_4\text{PtCl}_2$  (54–56% metallic Pt weight concentration, Thermofisher),  $(\text{NH}_4)_2\text{PtCl}_4$  (51% metallic Pt weight concentration, Thermofisher),  $(\text{NH}_4)_2\text{PtCl}_6$  (99.995% trace metals basis, Sigma-Aldrich) and ammonia hydroxide solution (28.0–30.0%, Sigma-Aldrich) were used without any additional purification. Fluorine-doped tin oxide (FTO) coated glass slides (coating thickness  $\approx 550$  nm, Pilkington) were cleaned by ultrasonication in acetone, ethanol, and deionized water for 15 min each, and silicon dioxide ( $\text{SiO}_2$ ) coated silicon (Si) wafers (Si thickness =  $380 \mu\text{m} \pm 25 \mu\text{m}$ ;  $\text{SiO}_2$

coating thickness = 100 nm, MicroChemicals GmbH) were pretreated by  $\text{O}_2$  plasma (SmartPlasma, Plasma technology GmbH). TEM supports (8 nm  $\text{SiO}_2$  membrane with  $\text{Si}_3\text{N}_4$  mesh on 200  $\mu\text{m}$  silicon; Ted Pella, Inc. and PELCO International) were purchased from Plano GmbH.

**$\text{TiO}_2$  Layer Fabrication:**  $\text{TiO}_2$  layers were formed on FTO and  $\text{SiO}_2$  substrates by DC magnetron sputtering (SP-P-US-6M-32 CreaTec Fischer & Co. GmbH), as previously described in literature.<sup>[72]</sup> First, Ti metal layers were sputtered under a vacuum using a 5” Ti target (99.995%, HMW Hauner GmbH & Co. KG) at 150 W for 10 s. Next, amorphous  $\text{TiO}_2$  layers were sputtered in an  $\text{Ar}:\text{O}_2$  atmosphere ( $6.7 \times 10^{-3}$  mbar; volume ratio  $\text{Ar}:\text{O}_2 = 10:5$ ) using the same Ti target at 500 W for 4 h to reach the thickness of 200 nm. Afterward, the coated substrates were annealed at 450 °C for 1 h in air to crystallize  $\text{TiO}_2$  layers.

For the purpose of transmission electron microscopy studies, 7 nm thin  $\text{TiO}_2$  layers were sputtered directly on TEM supports by DC magnetron sputtering at 500 W for 12 min, followed by annealing at 450 °C for 1 h in air.

**Pt Single Atom Deposition:** Pt single atoms (SA) were loaded on the surface of  $\text{TiO}_2$  layers by an adopted “reactive deposition” approach<sup>[61–65,68,101]</sup> using  $\text{H}_2\text{PtCl}_6 \cdot 6\text{H}_2\text{O}$  as a Pt source.  $\text{H}_2\text{PtCl}_6 \cdot 6\text{H}_2\text{O}$  solution (0.005 mM, 2 mM, or 10 mM) was prepared and transferred to the quartz cells, which were then purged with Ar gas to create anaerobic conditions.  $\text{TiO}_2$ -covered FTO supports were further immersed into the solutions and kept in dark in sealed quartz cells for 1 h. Upon completion, the supports were thoroughly rinsed with deionized water and dried with an  $\text{N}_2$  stream. In a reference experiment, 0.005 mM of  $(\text{NH}_4)_2\text{PtCl}_4$  or  $(\text{NH}_4)_2\text{PtCl}_6$  as a Pt source was used for reactive deposition. The pH of the  $(\text{NH}_4)_2\text{PtCl}_4$  solution was additionally adjusted to a value of 5.4, which was a similar value to initial pH of 0.005 mM  $\text{H}_2\text{PtCl}_6 \cdot 6\text{H}_2\text{O}$  solution.

For the Pt SAs deposited on  $\text{TiO}_2$  layers by SEA approach,  $(\text{NH}_3)_4\text{PtCl}_2$  aqueous solutions (0.005 mM or 10 mM concentration) were prepared. The pH of the  $(\text{NH}_3)_4\text{PtCl}_2$  solution was additionally adjusted to a value of 12.7 (or 10) by adding appropriate amounts of ammonia aqueous solution.  $\text{TiO}_2$ -coated substrates were subsequently immersed into the Ar-purged solutions for 1 h under dark conditions at room temperature. A series of Pt SAs-loaded samples were further subjected to thermal treatments in either air or  $\text{H}_2$  atmosphere at 250 °C or 400 °C for 1 h.

**Characterization:** High-angle annular dark-field scanning transmission electron microscopy (HAADF-STEM) images of the samples were acquired using a probe-corrected scanning transmission electron microscope (Thermo Fisher Scientific Spectra 200). Surface morphology of the samples was investigated by a field-emission scanning electron microscope (FE-SEM, S-4800, Hitachi). Composition and chemical state of the samples were analyzed by X-ray photoelectron spectroscopy (XPS, PHI 5600). XPS spectra were shifted to a standard Ti 2p binding energy in anatase of 458.5 eV. Peak deconvolution was carried out by MultiPak software.

**Electron Paramagnetic Resonance (EPR) Measurements:** EPR measurements were carried out for powdered  $\text{TiO}_2$  (nanosheets) loaded with Pt SAs via reactive deposition and strong electrostatic adsorption (SEA). Nanosheets were synthesized according to the reported method,<sup>[95]</sup> and then ultrasonically dispersed in either  $\text{H}_2\text{PtCl}_6$  or  $(\text{NH}_3)_4\text{PtCl}_2$  solutions and kept in dark for 1 h. Upon completion, the powders were collected and washed three times by centrifuging and rinsing with DI water and dried in air at 70 °C. The prepared Pt SAs-loaded powders (10 mg) were placed in quartz glass EPR tubes. EPR spectra were recorded on a JEOL continuous wave spectrometer JES-FA200, equipped with an X-band Gunn diode oscillator bridge, a cylindrical mode cavity, and a helium cryostat. The measurement setup was the following parameters:  $T = 95$  K, microwave frequency = 8.959 GHz, modulation width 1.0 mT, microwave power 1.0 mW, modulation frequency 100 kHz, and time constant of 0.1 s.

**Linear Sweep Voltammetry (LSV):** Linear sweep voltammetry studies were performed in a three-electrode electrochemical setup using platinum plate as a counter electrode, and an Ag/AgCl (3 M KCl) reference electrode. Polarization was carried out in dark in deaerated 0.1 M  $\text{Na}_2\text{SO}_4$  aqueous solutions by sweeping the potential in the cathodic direction from  $-0.2$  V to  $-1.5$  V (vs Ag/AgCl) with a scan rate of  $5 \text{ mV s}^{-1}$  using Autolab PG-STAT302N potentiostat/galvanostat.

**Photocatalytic H<sub>2</sub> Evolution:** Photocatalytic H<sub>2</sub> evolution performance of the Pt SAs/TiO<sub>2</sub> layers in aqueous solutions was evaluated under UV irradiation using methanol as a hole scavenger. The samples were placed in a quartz reactor containing 50 vol.% methanol aqueous solution (10 mL), which was then purged for 15 min with Ar, sealed, and illuminated for 3 h with an LED ( $\lambda = 365$  nm, power density of 65 mW cm<sup>-2</sup>, exposure area = 0.785 cm<sup>2</sup>). A gas chromatograph (GCMS-QO2010SE, SHIMADZU) with a thermal conductivity detector (TCD) was used to determine the amount of H<sub>2</sub> produced at specific time intervals.

## Supporting Information

Supporting Information is available from the Wiley Online Library or from the author.

## Acknowledgements

Y.W. and S.Q. contributed equally to this work. The authors would like to acknowledge DFG and the Operational Program Research, Development, and Education (European Regional Development Fund, Project No. CZ.02.1.01/0.0/0.0/15\_003/0000416 of the Ministry of Education, Youth, and Sports of the Czech Republic) for financial support, as well as the support of the Czech Science Foundation projects GA CR-EXPRO, 23–08019X. The authors would also like to acknowledge the support of the Center for Nanoanalysis and Electron Microscopy (CENEM, Friedrich-Alexander-Universität Erlangen-Nürnberg). BBS would like to thank the Deutsches Elektronen-Synchrotron for providing the beamtime. The authors would like to thank Dr. Edmund Welter, beamline scientist from P65, PETRA III, DESY, Hamburg, and Dr. Dmitry Doronkin, KIT for their help during the beamtime.

Open access funding enabled and organized by Projekt DEAL.

## Conflict of Interest

The authors declare that there is no conflict of interest.

## Data Availability Statement

The data that support the findings of this study are available from the corresponding author upon reasonable request.

## Keywords

highly reactive single-atom deposition, photocatalytic H<sub>2</sub> generations, Pt co-catalysts, sputtered anatase layers

Received: December 16, 2022

Revised: May 5, 2023

Published online:

- [1] Y. Chen, S. Ji, C. Chen, Q. Peng, D. Wang, Y. Li, *Joule* **2018**, 2, 1242.
- [2] H. Zhang, G. Liu, L. Shi, J. Ye, *Adv. Energy Mater.* **2018**, 8, 1701343.
- [3] S. Mitchell, J. Pérez-Ramírez, *Nat. Commun.* **2020**, 11, 4302.
- [4] D. Liu, Q. He, S. Ding, L. Song, *Adv. Energy Mater.* **2020**, 10, 2001482.
- [5] X. Li, X. Yang, Y. Huang, T. Zhang, B. Liu, *Adv. Mater.* **2019**, 31, 1902031.
- [6] Y. Zhou, J. Li, X. Gao, W. Chu, G. Gao, L.-W. Wang, *J. Mater. Chem. A* **2021**, 9, 9979.

- [7] Q. Zhang, J. Guan, *Adv. Funct. Mater.* **2020**, 30, 2000768.
- [8] C. Zhu, S. Fu, Q. Shi, D. Du, Y. Lin, *Angew. Chem.* **2017**, 56, 13944.
- [9] J. Su, R. Ge, Y. Dong, F. Hao, L. Chen, *J. Mater. Chem. A* **2018**, 6, 14025.
- [10] W. Zang, Z. Kou, S. J. Pennycook, J. Wang, *Adv. Energy Mater.* **2020**, 10, 1903181.
- [11] Q. Zhang, J. Guan, *Sol. RRL* **2020**, 4, 2000283.
- [12] Q. Wang, D. Zhang, Y. Chen, W.-F. Fu, X.-J. Lv, *ACS Sustainable Chem. Eng.* **2019**, 7, 6430.
- [13] J. Fu, S. Wang, Z. Wang, K. Liu, H. Li, H. Liu, J. Hu, X. Xu, H. Li, M. Liu, *Front. Phys.* **2020**, 15, 33201.
- [14] F. Zhang, Y. Zhu, Q. Lin, L. Zhang, X. Zhang, H. Wang, *Energy Environ. Sci.* **2021**, 14, 2954.
- [15] X. Chen, S. Shen, L. Guo, S. S. Mao, *Chem. Rev.* **2010**, 110, 6503.
- [16] A. J. Bard, *J. Photochem.* **1979**, 10, 59.
- [17] S. Bai, W. Yin, L. Wang, Z. Li, Y. Xiong, *RSC Adv.* **2016**, 6, 57446.
- [18] K. G. Pickup, B. M. W. Trapnell, *J. Chem. Phys.* **1956**, 25, 182.
- [19] S. Katz, G. B. Kistiakowsky, R. F. Steiner, *J. Am. Chem. Soc.* **1949**, 71, 2258.
- [20] W. V. Smith, *J. Chem. Phys.* **1943**, 11, 110.
- [21] J. Schneider, M. Matsuoka, M. Takeuchi, J. Zhang, Y. Horiuchi, M. Anpo, D. W. Bahnemann, *Chem. Rev.* **2014**, 114, 9919.
- [22] C. Dong, C. Lian, S. Hu, Z. Deng, J. Gong, M. Li, H. Liu, M. Xing, J. Zhang, *Nat. Commun.* **2018**, 9, 1252.
- [23] I. Vamvasakis, B. Liu, G. S. Armatas, *Adv. Funct. Mater.* **2016**, 26, 8062.
- [24] J. Ma, X. Tan, Q. Zhang, Y. Wang, J. Zhang, L. Wang, *ACS Catal.* **2021**, 11, 3352.
- [25] Y. Ben-Shahar, F. Scotognella, I. Kriegel, L. Moretti, G. Cerullo, E. Rabani, U. Banin, *Nat. Commun.* **2016**, 7, 10413.
- [26] F. Xue, C. Chen, W. Fu, M. Liu, C. Liu, P. Guo, S. Shen, *J. Phys. Chem. C* **2018**, 122, 25165.
- [27] C. Dessal, L. Martínez, C. Maheu, T. Len, F. Morfin, J. L. Rousset, E. Puzenat, P. Afanasiev, M. Aouine, L. Soler, J. Llorca, L. Piccolo, *J. Catal.* **2019**, 375, 155.
- [28] D. Riassetto, C. Holtzinger, M. Langlet, *J. Mater. Sci.* **2009**, 44, 2637.
- [29] S. Gutić, A. Dobrota, E. Fako, N. Skorodumova, N. López, I. Pašti, *Catalysts* **2020**, 10, 290.
- [30] M. Li, K. Duanmu, C. Wan, T. Cheng, L. Zhang, S. Dai, W. Chen, Z. Zhao, P. Li, H. Fei, Y. Zhu, R. Yu, J. Luo, K. Zang, Z. Lin, M. Ding, J. Huang, H. Sun, J. Guo, X. Pan, W. A. Goddard, P. Sautet, Y. Huang, X. Duan, *Nat. Catal.* **2019**, 2, 495.
- [31] K. Maiti, S. Maiti, M. T. Curnan, H. J. Kim, J. W. Han, *Adv. Energy Mater.* **2021**, 11, 2101670.
- [32] H. Hu, J. Wang, P. Tao, C. Song, W. Shang, T. Deng, J. Wu, *J. Mater. Chem. A* **2022**, 10, 5835.
- [33] Y. Chen, Z. Huang, Z. Ma, J. Chen, X. Tang, *Catal. Sci. Technol.* **2017**, 7, 4250.
- [34] J. T. Miller, M. Schreier, A. J. Kropf, J. R. Regalbuto, *J. Catal.* **2004**, 225, 203.
- [35] J. Sun, J. Zhang, H. Fu, H. Wan, Y. Wan, X. Qu, Z. Xu, D. Yin, S. Zheng, *Appl. Catal., B* **2018**, 229, 32.
- [36] X. Chen, X.-B. Wang, S. Han, D. Wang, C. Li, W. Guan, W.-Y. Li, C. Liang, *ACS Appl. Mater. Interfaces* **2022**, 14, 590.
- [37] M. Schneider, J. R. Regalbuto, *J. Catal.* **2004**, 225, 190.
- [38] J. E. Samad, S. Hoenic, J. R. Regalbuto, *ChemCatChem* **2015**, 7, 3460.
- [39] S. J. Tauster, S. C. Fung, R. L. Garten, *J. Am. Chem. Soc.* **1978**, 100, 170.
- [40] S. J. Tauster, *Acc. Chem. Res.* **1987**, 20, 389.
- [41] W. E. Kaden, T. Wu, W. A. Kunkel, S. L. Anderson, *Science* **2009**, 326, 826.
- [42] P. Liu, Y. Zhao, R. Qin, S. Mo, G. Chen, L. Gu, D. M. Chevrier, P. Zhang, Q. Guo, D. Zang, B. Wu, G. Fu, N. Zheng, *Science* **2016**, 352, 797.

- [43] T. Wang, Y. Zhu, Z. Luo, Y. Li, J. Niu, C. Wang, *Environ. Chem. Lett.* **2021**, *19*, 1815.
- [44] T. Wei, Y. Zhu, Y. Wu, X. An, L.-M. Liu, *Langmuir* **2019**, *35*, 391.
- [45] L. Chen, R. R. Unocic, A. S. Hoffman, J. Hong, A. H. Braga, Z. Bao, S. R. Bare, J. Szanyi, *JACS Au* **2021**, *1*, 977.
- [46] L. DeRita, S. Dai, K. Lopez-Zepeda, N. Pham, G. W. Graham, X. Pan, P. Christopher, *J. Am. Chem. Soc.* **2017**, *139*, 14150.
- [47] L. DeRita, J. Resasco, S. Dai, A. Boubnov, H. V. Thang, A. S. Hoffman, I. Ro, G. W. Graham, S. R. Bare, G. Pacchioni, X. Pan, P. Christopher, *Nat. Mater.* **2019**, *18*, 746.
- [48] J. P. Brunelle, *Pure Appl. Chem.* **1978**, *50*, 1211.
- [49] C. Conțescu, M. I. Vass, *Appl. Catal.* **1987**, *33*, 259.
- [50] T. Wang, X. Tao, X. Li, K. Zhang, S. Liu, B. Li, *Small* **2021**, *17*, 2006255.
- [51] S. Hoang, Y. Guo, A. J. Binder, W. Tang, S. Wang, J. J. Liu, H. Tran, X. Lu, Y. Wang, Y. Ding, E. A. Kyriakidou, J. Yang, T. J. Toops, T. R. Pauly, R. Ramprasad, P.-X. Gao, *Nat. Commun.* **2020**, *11*, 1062.
- [52] E. A. Kyriakidou, O. S. Alexeev, A. P. Wong, C. Papadimitriou, M. D. Amiridis, J. R. Regalbuto, *J. Catal.* **2016**, *344*, 749.
- [53] L. Jiao, J. R. Regalbuto, *J. Catal.* **2008**, *260*, 329.
- [54] L. Jiao, J. R. Regalbuto, *J. Catal.* **2008**, *260*, 342.
- [55] S. Chytil, W. R. Glomm, I. Kvande, T. Zhao, J. C. Walmsley, E. A. Blekkan, *Top. Catal.* **2007**, *45*, 93.
- [56] Y.-P. Qiu, Q. Shi, W.-Z. Wang, S.-H. Xia, H. Dai, H. Yin, Z.-Q. Yang, P. Wang, *Small* **2022**, *18*, 2106143.
- [57] B. Pongthawornsakun, N. Wimonsupakit, J. Panpranot, *J. Chem. Sci.* **2017**, *129*, 1721.
- [58] S. Lambert, N. Job, L. D'Souza, M. F. Ribeiro Pereira, R. Pirard, B. Heinrichs, J. L. Figueiredo, J.-P. Pirard, J. R. Regalbuto, *J. Catal.* **2009**, *261*, 23.
- [59] J. Xing, J. F. Chen, Y. H. Li, W. T. Yuan, Y. Zhou, L. R. Zheng, H. F. Wang, P. Hu, Y. Wang, H. J. Zhao, Y. Wang, H. G. Yang, *Chemistry* **2014**, *20*, 2138.
- [60] X. Zhou, I. Hwang, O. Tomanec, D. Fehn, A. Mazare, R. Zboril, K. Meyer, P. Schmuki, *Adv. Funct. Mater.* **2021**, *31*, 2102843.
- [61] Z. Wu, I. Hwang, G. Cha, S. Qin, O. Tomanec, Z. Badura, S. Kment, R. Zboril, P. Schmuki, *Small* **2022**, *18*, 2104892.
- [62] Y. Wang, I. Hwang, Z. Wu, P. Schmuki, *Electrochem. Commun.* **2021**, *133*, 107166.
- [63] S. Hejazi, S. Mohajernia, B. Osuagwu, G. Zoppellaro, P. Andryskova, O. Tomanec, S. Kment, R. Zbořil, P. Schmuki, *Adv. Mater.* **2020**, *32*, 1908505.
- [64] G. Cha, I. Hwang, S. Hejazi, A. S. Dobrota, I. A. Pašti, B. Osuagwu, H. Kim, J. Will, T. Yokosawa, Z. Badura, Š. Kment, S. Mohajernia, A. Mazare, N. V. Skorodumova, E. Spiecker, P. Schmuki, *iScience* **2021**, *24*, 102938.
- [65] G. Cha, A. Mazare, I. Hwang, N. Denisov, J. Will, T. Yokosawa, Z. Badura, G. Zoppellaro, A. B. Tesler, E. Spiecker, P. Schmuki, *Electrochim. Acta* **2022**, *412*, 140129.
- [66] I. Hwang, A. Mazare, J. Will, T. Yokosawa, E. Spiecker, P. Schmuki, *Adv. Funct. Mater.* **2022**, *32*, 2207849.
- [67] S. Qin, N. Denisov, B. B. Sarma, I. Hwang, D. E. Doronkin, O. Tomanec, S. Kment, P. Schmuki, *Adv. Mater. Interfaces* **2022**, *9*, 2200808.
- [68] S. Qin, N. Denisov, J. Will, J. Kolařík, E. Spiecker, P. Schmuki, *Sol. RRL* **2022**, *6*, 2101026.
- [69] S.-M. Wu, I. Hwang, B. Osuagwu, J. Will, Z. Wu, B. B. Sarma, F.-F. Pu, L.-Y. Wang, Z. Badura, G. Zoppellaro, E. Spiecker, P. Schmuki, *ACS Catal.* **2023**, *13*, 33.
- [70] X. Hu, J. Song, J. Luo, H. Zhang, Z. Sun, C. Li, S. Zheng, Q. Liu, *J. Energy Chem.* **2021**, *62*, 1.
- [71] S. Weon, M.-J. Suh, C. Chu, D. Huang, E. Stavitski, J.-H. Kim, *ACS EST Eng* **2021**, *1*, 512.
- [72] H. Kim, Y. Wang, N. Denisov, Z. Wu, Š. Kment, P. Schmuki, *J. Mater. Sci.* **2022**, *57*, 12960.
- [73] J. F. Lambert, E. Marceau, B. Shelimov, J. Lehman, V. L. e. Bel de Penguilly, X. Carrier, S. Boujday, H. Pernot, M. Che, *Stud. Surf. Sci. Catal.* **2000**, *130*, 1043.
- [74] M. Kosmowski, *Adv. Colloid Interface Sci.* **2002**, *99*, 255.
- [75] S. Kuhadomlap, O. Mekasuwandumrong, P. Praserttham, S.-I. Fujita, M. Arai, J. Panpranot, *Catalysts* **2018**, *8*, 87.
- [76] J. Xi, X. Zhang, X. Zhou, X. Wu, S. Wang, W. Yu, N. Yan, K. P. Loh, Q.-H. Xu, *J. Colloid Interface Sci.* **2022**, *623*, 799.
- [77] A. Naldoni, M. Altomare, G. Zoppellaro, N. Liu, Š. Kment, R. Zbořil, P. Schmuki, *ACS Catal.* **2019**, *9*, 345.
- [78] S. Livraghi, M. Chiesa, M. C. Paganini, E. Giamello, *J. Phys. Chem. C* **2011**, *115*, 25413.
- [79] F. Pellegrino, E. Morra, L. Mino, G. Martra, M. Chiesa, V. Maurino, *J. Phys. Chem. C* **2020**, *124*, 3141.
- [80] Y. Akdogan, C. Vogt, M. Bauer, H. Bertagnolli, L. Giurgiu, E. Roduner, *Phys. Chem. Chem. Phys.* **2008**, *10*, 2952.
- [81] J. R. Katzer, G. C. A. Schuit, J. H. C. Van Hooff, *J. Catal.* **1979**, *59*, 278.
- [82] A. Munoz-Paez, D. C. Koningsberger, *J. Phys. Chem.* **1995**, *99*, 4193.
- [83] G. Jantelot, M. Qureshi, M. Harb, S. Ould-Chikh, D. H. Anjum, E. Abou-Hamad, A. Aguilar-Tapia, J.-L. Hazemann, K. Takanabe, J.-M. Basset, *Phys. Chem. Chem. Phys.* **2019**, *21*, 24429.
- [84] S. Qin, J. Will, H. Kim, N. Denisov, S. Carl, E. Spiecker, P. Schmuki, *ACS Energy Lett.* **2023**, *8*, 1209.
- [85] W. A. Spieker, J. Liu, J. T. Miller, A. J. Kropf, J. R. Regalbuto, *Appl. Catal., A* **2002**, *232*, 219.
- [86] E. H. Archibald, *J. Chem. Soc., Trans.* **1920**, *117*, 1104.
- [87] C. M. Davidson, R. F. Jameson, *Trans. Faraday Soc.* **1965**, *61*, 2462.
- [88] R. Dreyer, J. Dreyer, *Z. Chem.* **1963**, *3*, 151.
- [89] R. Dreyer, I. Dreyer, D. Rettig, *Z. Phys. Chem.* **1963**, *2240*, 199.
- [90] X. Zhang, Z. Li, W. Pei, G. Li, W. Liu, P. Du, Z. Wang, Z. Qin, H. Qi, X. Liu, S. Zhou, J. Zhao, B. Yang, W. Shen, *ACS Catal.* **2022**, *12*, 3634.
- [91] T. Lee, *J. Catal.* **1984**, *90*, 279.
- [92] J. Cai, A. Cao, Z. Wang, S. Lu, Z. Jiang, X.-Y. Dong, X. Li, S.-Q. Zang, *J. Mater. Chem. A* **2021**, *9*, 13890.
- [93] R. T. K. Baker, E. B. Prestidge, R. L. Garten, *J. Catal.* **1979**, *59*, 293.
- [94] S. Wei, A. Li, J.-C. Liu, Z. Li, W. Chen, Y. Gong, Q. Zhang, W.-C. Cheong, Y. Wang, L. Zheng, H. Xiao, C. Chen, D. Wang, Q. Peng, L. Gu, X. Han, J. Li, Y. Li, *Nat. Nanotechnol.* **2018**, *13*, 856.
- [95] N. Denisov, S. Qin, J. Will, B. N. Vasiljevic, N. V. Skorodumova, I. A. Pašti, B. B. Sarma, B. Osuagwu, T. Yokosawa, J. Voss, J. Wirth, E. Spiecker, P. Schmuki, *Adv. Mater.* **2023**, *35*, 2206569.
- [96] M. S. Heise, J. A. Schwarz, *J. Colloid Interface Sci.* **1985**, *107*, 237.
- [97] M. S. Heise, J. A. Schwarz, *J. Colloid Interface Sci.* **1986**, *113*, 55.
- [98] M. S. Heise, J. A. Schwarz, *J. Colloid Interface Sci.* **1988**, *123*, 51.
- [99] J. A. Schwarz, M. S. Heise, *J. Colloid Interface Sci.* **1990**, *135*, 461.
- [100] X. Cheng, Y. Li, L. Zheng, Y. Yan, Y. Zhang, G. Chen, S. Sun, J. Zhang, *Energy Environ. Sci.* **2017**, *10*, 2450.
- [101] Y. Chen, S. Ji, W. Sun, Y. Lei, Q. Wang, A. Li, W. Chen, G. Zhou, Z. Zhang, Y. Wang, L. Zheng, Q. Zhang, L. Gu, X. Han, D. Wang, Y. Li, *Angew. Chem.* **2020**, *132*, 1311.